Stable and metastable structures of the multiphase tantalum nitride system

C. Stampfl[1] and A. J. Freeman[2]
[1]*School of Physics, The University of Sydney, Sydney 2006 Australia*
[2]*Department of Physics and Astronomy, Northwestern University, Evanston, Illinois, 60208, USA*
(Received 14 May 2004; revised manuscript received 10 September 2004; published 20 January 2005)

Despite its growing technological importance and potential, the tantalum nitride system is suprisingly still relatively unexplored. Using density functional theory and the all-electron total energy full-potential linearized augmented plane-wave method, we investigate the relative stability of a host of structural phases and their associated electronic properties. Through consideration of the effect of the environment via the individual atom chemical potentials, a phase diagram is obtained. Our calculations indicate that there are three *stable* phases Ta_5N_6, Ta_2N, and Ta_3N_5—the rest being metastable. The close energies of many structures explains the complexity of this nitride materials system and why the observed structural phases depend very sensitively upon experimental synthesis and growth conditions.

DOI: 10.1103/PhysRevB.71.024111 PACS number(s): 71.20.Be

While the tantalum nitride system is attracting much interest recently due to its potential for technological applications, it remains largely unexplored both experimentally and theoretically. It exhibits a remarkable richness with regard to the array of equilibrium and metastable phases that can form[1,2] and is used, for example, in coatings for cutting tools and wear-resistant layers, as well as for thin-film resistors and diffusion barriers in integrated circuits.[3] More recently, it has been the subject of growing investigations regarding its potential as an electronic material, particularly as a barrier layer in Josephson junctions, which consist of superconductor/normal-conductor/superconductor (SNS) interfaces—devices that are of great interest in connection with high-speed digital electronics.[4] An optimum performance of the SNS junction $NbN/TaN_x/NbN$ has been reported when TaN_x has a resistivity close to the metal-insulator (M-I) transition; there it was demonstrated that the resistivity can be *tuned* by the growth conditions—namely, by the nitrogen pressure and the temperature.[5–9] The experiments indicated that at the M-I transition, the material has a N-rich stoichiometry and that the rocksalt structure is essentially maintained. In order to shed light on the underlying mechanism responsible for the transition, we investigated *defective* N-rich rocksalt TaN structures.[6,10] Our results suggested that Ta vacancies are directly related to the above-mentioned M-I transition.

Other experiments have also been performed on this materials system: Using dc magnetron sputtering on silicon $\langle 001 \rangle$ substrates, where the ratio of Ta to N atoms in the plasma could be controlled, Lu *et al.*[8] observed the formation of pure Ta, γ-Ta_2N, δ-TaN, and Ta_5N_6 phases which have increasing N content; concominantly, the resistivity was found to increase. In these experiments, the working pressure was 2.5×10^{-3} Torr ($\sim3.3\times10^{-6}$ atm) and an annealing temperature of 600 °C (873 K) was used. In the early work of Terao,[2] many phases were reported which were formed by nitriding evaporated Ta films in an atmosphere of ammonia and nitrogen. Temperatures in the range of 600–1100 °C (873–1375 K) were employed to achieve the $TaN_{\sim0.5}$, Ta_2N, δ-TaN, ϵ-TaN, Ta_5N_6, Ta_4N_5, and Ta_3N_5 phases. It was found that on heating the thin films of Ta_3N_5 in vacuum, the phase transformations $Ta_3N_5 \rightarrow Ta_4N_5 \rightarrow Ta_5N_6 \rightarrow \epsilon$-TaN $\rightarrow Ta_2N$ resulted as the N content decreased. Using ultrahigh-vacuum reactive magnetron sputtering of Ta as a function of the N_2 pressure over MgO(001) and oxidized Si(001), a series of lower nitrides ($TaN_{0.1}$, Ta_4N, Ta_2N) was observed by Shin *et al.*[1] for low pressures; for higher N_2 pressures and temperatures of 566–634 °C (823–923 K), a mixture of rocksalt TaN_x and body-centered-tetragonal TaN_x structures were observed.

It can be noted from these experiments that TaN compounds have widely varying structural properties, which depend sensitively on the experimental procedures and conditions. While this flexibility and control thereof raises the possibility of new, diverse applications, it is first necessary to gain a deeper understanding into the energetics and physical properties of these materials.

In the present paper, through density functional theory and the concept of the atom chemical potential, we investigate the relative stability and associated properties of a host of Ta-N structures—namely, tetragonal Ta_4N_5,[2,11] orthorhombic Ta_3N_5,[2,12] hexagonal Ta_5N_6,[2] hexagonal γ-Ta_2N,[2] hexagonal ϵ-TaN,[2] and cubic rocksalt δ-TaN,[11] as well as an array of rocksalt structures containing native defects. From the calculated energies, we construct a phase diagram which reveals the formation of stable and metastable phases, thus providing new understanding into the general behavior of this interesting nitride system.

The density functional theory (DFT) calculations were performed using the first-principles full-potential linearized augmented plane-wave (FLAPW) method[13,14] with the local density approximation[15] (LDA) for the exchange-correlation potential. We treat the core states fully relativistically and the valence states scalar relativistically and use angular momenta up to $l=8$ in the muffin-tin spheres for both the wave functions and charge density in the self-consistent cycles. The energy cutoff for the plane-wave expansion in the interstitial region between the muffin-tin spheres is taken to be 20.25 Ry, and the muffin-tin radii employed are $R_N=1.4$ Bohr for N and $R_{Ta}=2.47$ Bohr for Ta, except for the N interstitials and the Ta_3N_5 phase where, due to the smaller N-Ta dis-

TABLE I. The heat of formation per atom, $E^f(\mu_{\mathrm{Ta}}^0,\mu_{\mathrm{N}}^0)=[E_{\mathrm{sys}}^{\mathrm{total}}-n\mu_{\mathrm{Ta}}^0-m\mu_{\mathrm{N}}^0]/(m+n)$ where $E_{\mathrm{sys}}^{\mathrm{total}}$ is the total energy of the particular Ta_xN_y structure calculated using the supercell, and n and m are the number of Ta and N atoms in the supercell, respectively. μ_{N}^0 and μ_{Ta}^0 are the N- and Ta-atom chemical potentials, corresponding to the free nitrogen molecule and bulk bcc Ta, respectively. The units are eV.

rs-Ta_4N_3 (one N vac.)	Ta_4N_5	Ta_3N_5	rs-Ta_3N_4 (one Ta vac.)	rs-TaN	rs-Ta_4N_2 (two N vac.)	ϵ-TaN	hex-Ta_2N	Ta_5N_6
−1.297	−1.503	−1.478	−1.421	−1.305	−1.051	−1.117	−1.086	−1.658

tances, we used $R_{\mathrm{Ta}}=2.10$ bohr and $R_{\mathrm{Ta}}=2.2$ bohr, respectively. In the calculation of *energy differences*, we took care to use exactly the same plane-wave cutoff and muffin-tin radii and, as close as possible, **k**-point samplings.

To compare the relative stabilities of the various structures (see Table I), we define the free energy of formation

$$E^f(\mu_{\mathrm{Ta}},\mu_{\mathrm{N}}) \approx \left[E_{\mathrm{sys}}^{\mathrm{total}} - n\mu_{\mathrm{Ta}} - m\mu_{\mathrm{N}}\right]/(m+n), \qquad (1)$$

where $E_{\mathrm{sys}}^{\mathrm{total}}$ is the total energy of the Ta-N system calculated using the supercell and n and m are the number of Ta and N atoms in the supercell, respectively. Here, μ_{N} and μ_{Ta} are the N- and Ta-atom chemical potentials, respectively. The temperature enters through the dependence of the nitrogen chemical potential as given in Eq. (2). The $\approx$sign indicates that we ignore the entropic differences between the different structures. According to Eq. (1), a given structure will become *unstable* for combinations of μ_{Ta} and μ_{N} which give $E^f(\mu_{\mathrm{Ta}},\mu_{\mathrm{N}}) \geqslant 0$; that is, the structure becomes *endothermic*. For $\mu_{\mathrm{N}}=1/2E_{\mathrm{N_2}}^{\mathrm{total}}$ (half the total energy of an N_2 molecule), we call this the "nitrogen-rich" condition and choose it as the zero reference state (μ_{N}^0) of μ_{N} (cf., Fig. 4 below). Similarly, for $\mu_{\mathrm{Ta}}=E_{\mathrm{Ta\text{-}bulk}}^{\mathrm{total}}$ (the total energy of bulk, bcc Ta), we call this the "tantalum-rich" condition, and we choose it to be the zero reference state (μ_{Ta}^0) of μ_{Ta}. That is, in Fig. 4 (below), the values of the chemical potentials are given with respect to (μ_{N}^0,μ_{Ta}^0). The tantalum-rich state will be approached when there are excessive Ta atoms in the system compared to nitrogen molecules and the nitrogen-rich state when there are excessive N_2 molecules in the system as compared to Ta atoms.

The N chemical potential is dependent on the N_2 gas pressure and temperature through

$$\mu_{\mathrm{N}}(T,p_{\mathrm{N_2}}) = \frac{1}{2}\left[E_{\mathrm{N_2}}^{\mathrm{total}} + \tilde{\mu}_{\mathrm{N}}(T,p^0) + k_{\mathrm{B}}T\ln\left(\frac{p_{\mathrm{N_2}}}{p^0}\right)\right], \qquad (2)$$

as obtained by manipulation of the ideal gas equations.[16] Here $p_{\mathrm{N_2}}$ is the nitrogen pressure, p^0 corresponds to atmospheric pressure, and k_{B} is the Boltzmann constant. The temperature dependence of $\tilde{\mu}_{\mathrm{N}}(T,p^0)$ in the standard state (1 atm), which describes the contribution from rotations and vibrations of the molecule, as well as the ideal-gas entropy, is taken from tabulated thermodynamic data.[17]

We first consider the electronic properties of the phases which form in nature, noting that although they have been identified experimentally, they may not necessarily be *stable* (equilibrium) structures. The atomic geometry of rocksalt TaN is shown in Fig. 1(a), along with the electron density of states (DOS) [Fig. 1(b)] which shows clearly that TaN is metallic. The calculated equilibrium volume is 1.0% smaller than experiment. The Ta_4N_5 phase, depicted in Figs. 1(c) and 1(d), also has the rocksalt structure, but contains an ordered arrangement of Ta vacancies.[11] There are 18 atoms in the unit cell. The calculated equilibrium volume of Ta_4N_5 is 1.2% smaller than the experimental value. The corresponding DOS [Fig. 1(e)] exhibits a noticeable dip at E_F, suggesting a greater stability as compared to TaN. The electronic structure of these phases was presented and discussed in more detail in our earlier publication (Ref. 10).

The structure of the Ta_3N_5 phase (tritantalum pentanitride) is displayed in Figs. 2(a) and 2(b). Each Ta atom is surrounded by six N atoms, and the N atoms are threefold and fourfold Ta coordinated.[12] The optimized volume is found to be just 0.1% smaller than experiment. There are 32 atoms in the unit cell. The corresponding DOS [Fig. 2(c)]

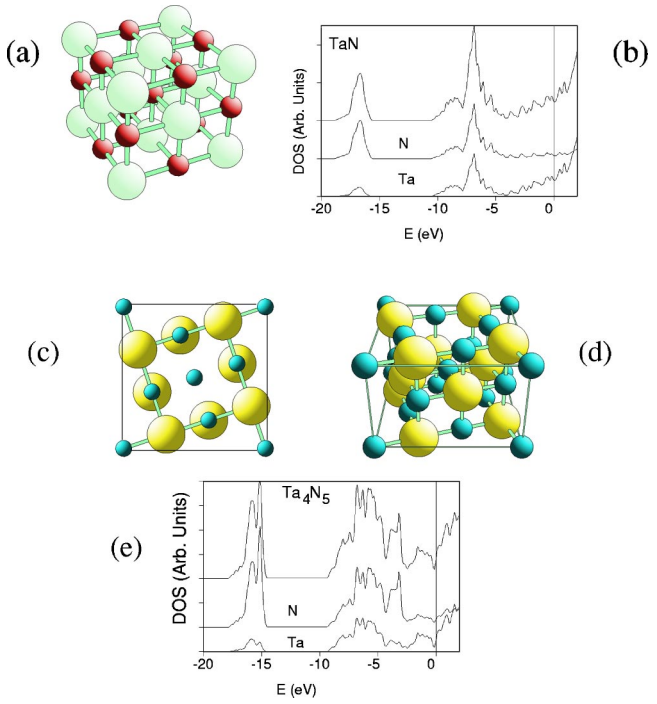

FIG. 1. (Color online) (a) Perspective view of the structure of rocksalt TaN. (b) Corresponding total (upper curve) and partial (Ta and N) density of states (DOS). Structure of Ta_4N_5: (c) view of the (001) plane and (d) perspective view. The large pale and small dark balls represent Ta and N atoms, respectively. The unit cell is indicated by the lines. (e) Corresponding total DOS (upper curve) and partial (Ta and N) DOS as indicated; the vertical line at zero energy indicates the Fermi level.

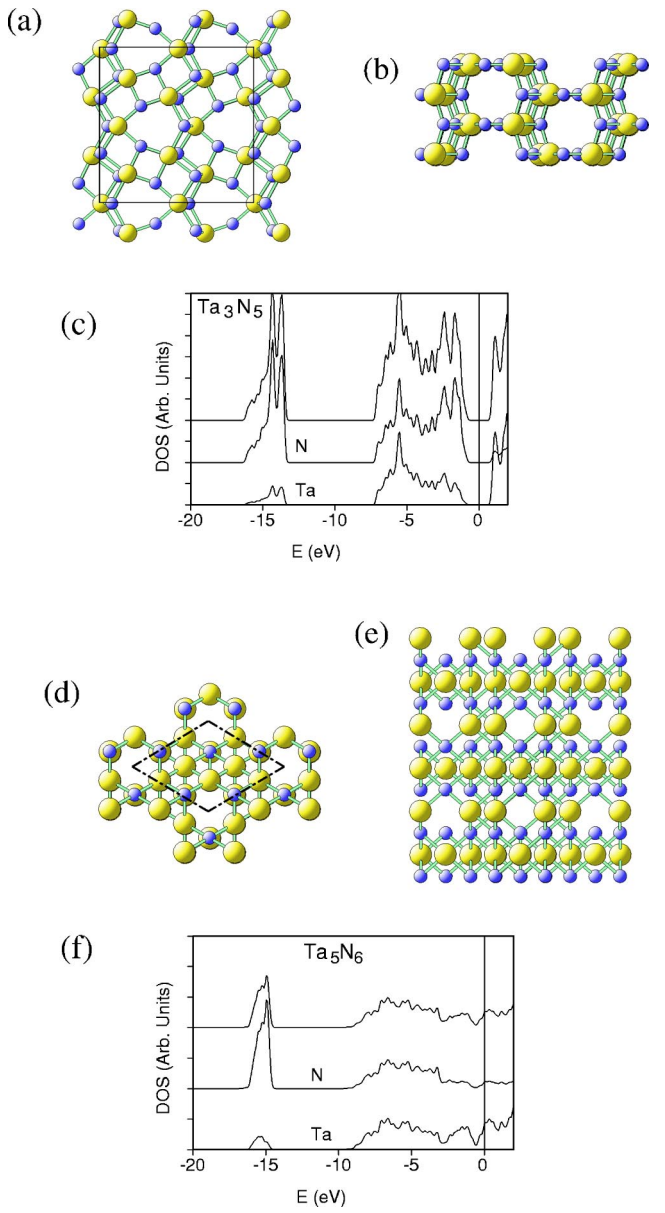

FIG. 2. (Color online) Structure of Ta_3N_5: (a) view of the (001) plane where the unit cell is indicated and (b) view of the (100) plane. (c) Total density of states (DOS) and partial (Ta and N) DOS. Atomic geometry of the Ta_5N_6 structure: (d) view of the (0001) plane with the unit cell indicated by the dot-dashed lines, and (e) side view. (f) Corresponding total DOS of Ta_5N_6 (upper curve) and partial (Ta and N) DOS. The large pale and small dark balls represent Ta and N atoms, respectively. The vertical line in the DOS at zero energy marks the Fermi level.

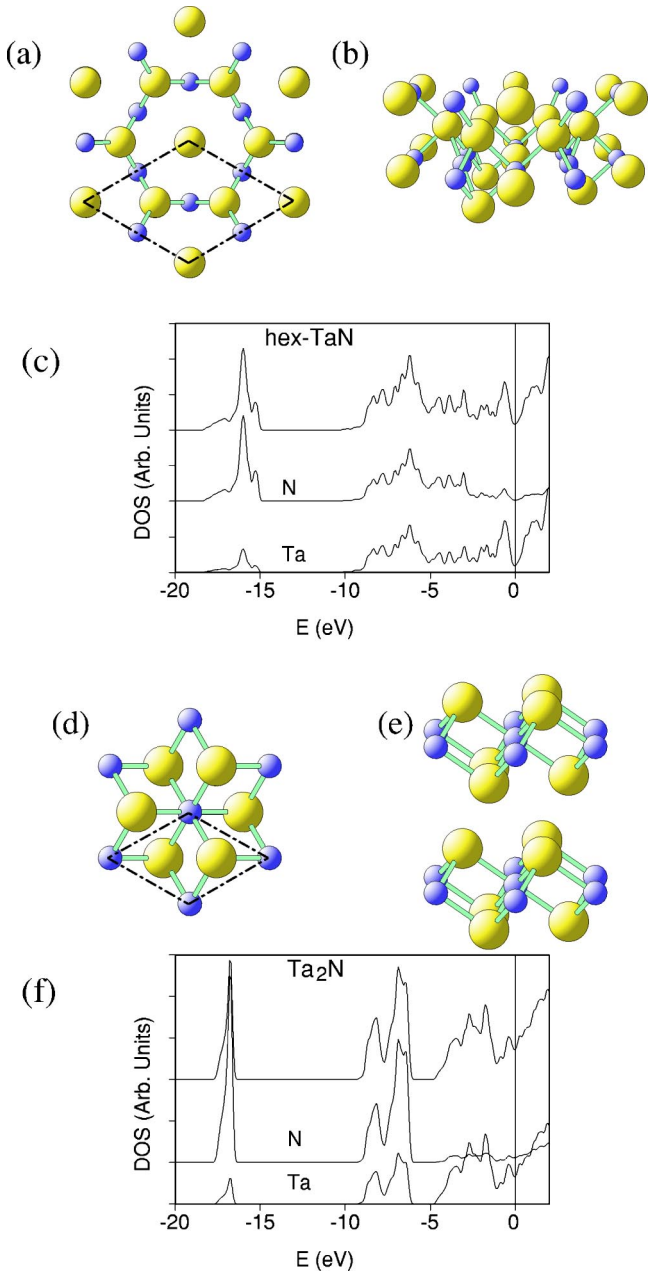

FIG. 3. (Color online) Structure of hexagonal ϵ-TaN: (a) view of the (0001) plane and (b) perspective view. The unit cell is indicated by the dot-dashed lines. (c) Total and partial (Ta and N) DOS. Structure of hexagonal Ta_2N: (d) view of the (0001) plane and (e) perspective view. The unit cell is indicated by the dot-dashed lines. (f) Total and partial (Ta and N) DOS of Ta_2N. The large pale and small dark balls represent Ta and N atoms, respectively. The vertical line in the DOS at zero energy indicates the Fermi level.

(Ref. 10) shows that the material is *insulating*—i.e., a semiconductor with a band gap of 1.5 eV. We note that in reality the band gap will be larger due to the well-known underestimation of the LDA. A more accurate description of the band gap could be obtained by performing quasiparticle calculations using the GW approximation to the self energy,[18] screened-exchange (SX) LDA,[19] self-interaction corrected (SIC),[20] or exact-exchange[21] calculations.

We turn now to the hexagonal phases. The atomic geometry of Ta_5N_6 is depicted in Figs. 2(d) and 2(e). The close-packed N layers follow the stacking sequence *ABAC* with Ta atoms and tantalum vacancies in the octahedral holes. The calculated equilibrium volume is 2.6% smaller than experiment. There are 22 atoms in the unit cell. The DOS shows that the material is metallic and that there is a strong hybridization between N and Ta atoms in the valence band region. The stoichiometric hexagonal ϵ-TaN phase is shown in Figs. 3(a) and 3(b). There are six atoms in the unit cell. The cal-

culated equilibrium volume is 0.7% less than the experimental value. From the DOS [Fig. 3(c)] it can be seen that there is also strong hybridization between N and Ta atoms in the valence band region. Finally, the atomic geometry of hexagonal Ta_2N is presented in Figs. 3(d) and 3(e). There are just three atoms in the unit cell. The equilibrium volume is calculated to be 0.6% smaller than experiment. The DOS shows clearly that this material is metallic; it can furthermore be seen from the partial DOS that the states above -5 eV are largely Ta derived.

In addition to these phases which have been observed in nature, we performed calculations for many defective rock-salt structures: namely, different concentrations of Ta and N vacancies, N interstitials, and N antisites. In general, we found that material with lower Ta concentrations had a relatively lower DOS at the Fermi level, which implies an increased resistivity. The results were reported in Ref. 10. In the present work, we consider (below) only the lowest energy of these defects, which are the N and Ta vacancies.

Having discussed the atomic and electronic properties of the various Ta-N structures, we now consider their *relative stability*. In Fig. 4(a), the free energy of formation [cf. Eq. (1)] is shown as a function of μ_N (keeping fixed $\mu_{Ta}=\mu_{Ta}^0=E_{Ta\text{-bulk}}^{total}$), and in Fig. 4(b), the analogous result is presented, but as a function of μ_{Ta} (keeping fixed $\mu_N=\mu_N^0=1/2E_{N_2}^{total}$). It can be seen clearly that the Ta_5N_6 phase is the most stable for a wide range of the chemical potentials. For strongly N-poor conditions (more negative values of μ_N), the Ta_2N phase becomes stable, while for strongly Ta-poor conditions (more negative values of μ_{Ta}) the insulating Ta_3N_5 phase becomes stable. Thus, even though many structures and phases have been identified experimentally, the calculations indicate that only three are stable and the rest are *metastable*. Furthermore, it is quite remarkable that for the full range of chemical potentials shown in Fig. 4(a), all nine Ta-N structures lie within just 0.5 eV of each other—and at $\mu_N \approx -1.5$ eV, seven lie within less than 0.13 eV of one another. This suggests that the behavior of the system (i.e., the actual structures observed) will depend very sensitively on the experimental procedures and the conditions or "environment" in which the material is held. For example, if there is insufficient atomic rearrangement possible due to diffusion barriers, then structures with a higher energy may be realized; i.e., the formation of energetically more favorable phases may be *kinetically hindered* under certain conditions. These results are indeed in line with the various experimental results and help explain why a large array of different phases have been observed. We note, as mentioned above, the present results are based on ground-state electronic structure calculations and do not take into account entropy effects of the bulk systems. Such effects could somewhat affect the relative energies of the structures when such small differences are involved.

Each of the lines in Figs. 4(a) and 4(b) becomes a plane in (μ_N, μ_{Ta}) space. Considering the planes corresponding to the structures with the *lowest* energy for a given (μ_N,μ_{Ta}), we obtain the phase diagram shown in Fig. 4(c). The unshaded region corresponds to that where there are no stable or metastable structures; i.e., all are unstable. As suggested by Figs. 4(a) and 4(b), the Ta_5N_6 phase dominates the phase diagram,

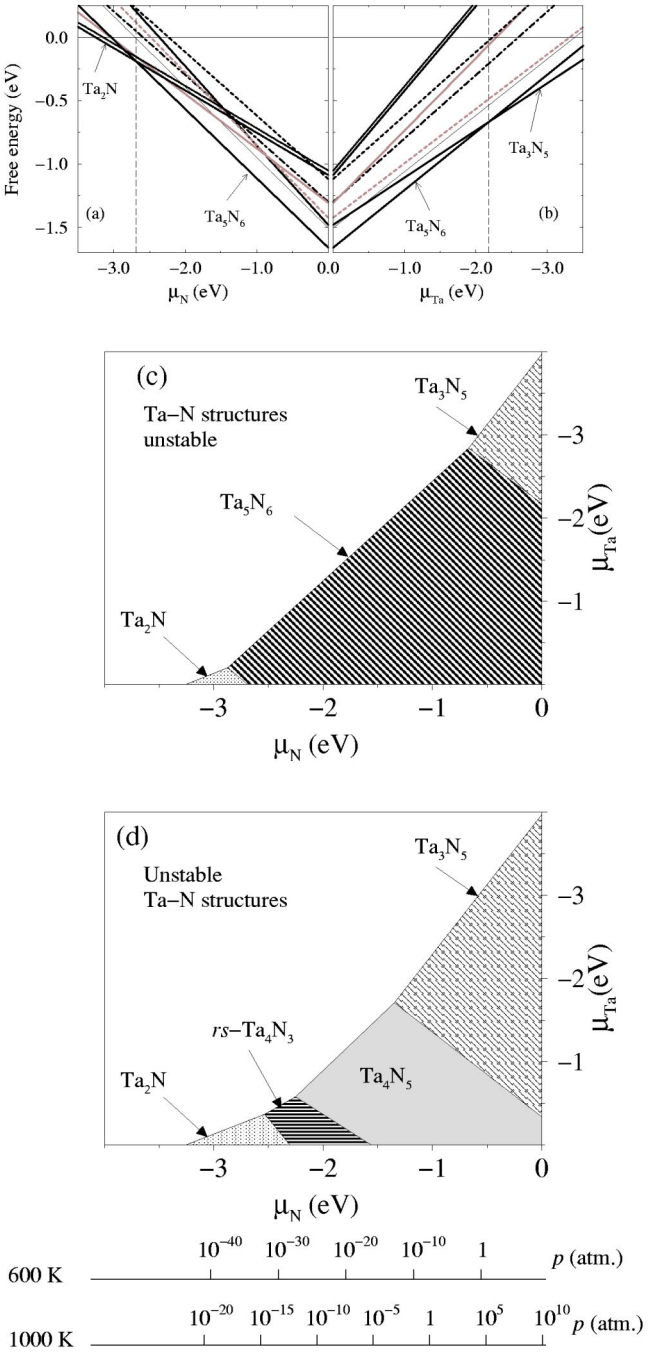

FIG. 4. The free energy of formation per atom: (a) as a function of μ_N for fixed $\mu_{Ta}=\mu_{Ta}^0=E_{Ta-bulk}^{total}$ and (b) as a function of μ_{Ta} for fixed $\mu_N=\mu_N^0=1/2E_{N_2}^{total}$. The lines represent the following structures: thick black, Ta_5N_6 (labeled); thick black, hex-Ta_2N (labeled); thick black, Ta_3N_5 (labeled); thin black, Ta_4N_5; thick dot-dashed, rs-TaN; thick dashed, ϵ-TaN; thick dotted, rs-Ta_4N_2 (two N vacancies); thick gray rs-Ta_4N_3 (one N vacancy); and thick dashed gray rs-Ta_3N_4 (one Ta vacancy). The vertical lines guide the eye for the stability region of the stable phases. (c) The phase diagram showing the stable structures as a function of the atom chemical potentials. (d) Resulting phase diagram when omitting the most stable Ta_5N_6 structure. For Figs. 4(c) and 4(d), the pressure range corresponding to μ_N [cf. Eq. (2)] is shown for two selected temperatures.

with only two other phases being stable: namely, Ta_2N for low values of μ_N and high values of μ_{Ta}, and Ta_3N_5 for the opposite extremes.

It is interesting to consider the phase diagram that results if we exclude the Ta_5N_6 phase (e.g., if it is prevented from forming due to particular experimental conditions). The result is shown in Fig. 4(d). In this case, in addition to the Ta_2N and Ta_3N_5 phases, which are now favorable over a larger region, the Ta_4N_5 structure appears in a relatively wide range of (μ_N,μ_{Ta}) phase space and, in addition, a structure containing N vacancies in a rocksalt lattice is seen (rs-Ta_4N_3). It can be noticed that when sweeping from right to left in the phase diagram and going from high μ_N, low μ_{Ta} to more low μ_N, high μ_{Ta} conditions, the Ta to N ratio increases; namely, it changes from 0.6 (Ta_3N_5) to 0.8 (Ta_4N_5) to 1.33 (rs-Ta_4N_3) to 2.0 (Ta_2N); that is, the phases change from so-called "higher nitrides" to "lower nitrides." This is similar to the trend found in Ref. 2 when heating the Ta_3N_5 phase under UHV as described in the Introduction, which causes desorption and loss of N atoms as N_2, resulting in progressively more Ta-rich materials.

In Figs. 4(c) and 4(d), the scale of the N chemical potential is correlated with the N_2 pressure for two selected temperatures [cf. Eq. (2)]. At 600 K, it can be seen from Fig. 4(c) that for pressure ranges used in industry and laboratories—i.e., from ultrahigh vacuum to 100 atm (10^{-15}–100 atm or 0.65×10^{-12}–0.65×10^{5} Torr), which correspond to μ_N in the range of ~-0.4 to ~-1.4 eV, the Ta_5N_6 phase is the most stable. This is also the case at 1000 K even though the corresponding range of μ_N is shifted and considerably extended (~-0.8 to ~-2.4 eV). Considering Fig. 4(d), however, which contains the metastable N-vacancy structure (rs-Ta_4N_3) and Ta_4N_5 phase, it can be seen that at 600 K, Ta_4N_5 is favored, while at 1000 K, depending on the pressure, either Ta_4N_5, rs-Ta_4N_3, or even Ta_2N may be favored. Thus, through variation of the temperature and pressure, different structures become energetically favored, and in general, structures with higher N contents are predicted for higher N_2 pressures, while for a given pressure, higher temperatures are predicted to give rise to more N-deficient structures. This is in qualitative agreement with the experimental results.[5,6]

In summary, through highly precise total energy FLAPW calculations we studied the relative stability and associated electronic properties of stable and metastable structures of the Ta-N system. In all cases, the calculated equilibrium volume is in excellent agreement with experiment. We find that there are three stable phases—namely, Ta_2N, Ta_5N_6, and Ta_3N_5; the rest are metastable. The electronic properties range from strongly metallic (Ta_2N) to more resistive (Ta_5N_6) and finally to insulating (Ta_3N_5). The very close energies calculated for the various structures investigated for certain regions of the phase diagram suggest that kinetic effects (due, e.g., to diffusion barriers for atomic rearrangement or epitaxial stabilization effects) will play an important role for this complex system and that the chemical and phase compositions of deposited films will depend critically on the growth conditions. This is in accordance with, and helps explain, the wide range of different structures observed experimentally.

ACKNOWLEDGMENTS

This work was supported by DARPA (Grant No. N00014-02-1-0598) and computing resources provided at the Artic Region Supercomputing Center. We thank Nate Newman for stimulating discussions.

[1] C.-S. Shin, Y.-W. Kim, D. Gall, J. E. Greene, and I. Petrov, Thin Solid Films **402**, 172 (2002).
[2] N. Terao, Jpn. J. Appl. Phys. **10**, 248 (1971).
[3] M. H. Tsai, S. C. Sun, C. P. Lee, H. T. Chiu, C. E. Tsai, S. H. Chuang, and S. C. Wu, Thin Solid Films **270**, 531 (1995).
[4] K. Likharev, Phys. World **10**(5), 39 (1997).
[5] A. B. Kaul, L. Yu, N. Newman, J. M. Rowell, S. R. Whiteley, and T. Van Duzer, Appl. Phys. Lett. **78**, 99 (2001).
[6] L. Yu, C. Stampfl, D. Marshall, T. Eshrich, V. Narayanan, J. M. Rowell, N. Newman, and A. J. Freeman, Phys. Rev. B **65**, 245110 (2002).
[7] O. Yu. Khyzhun and Y. V. Zaulchny, Phys. Status Solidi B **207**, 191 (1998).
[8] Y. M. Lu, R. J. Weng, W. S. Hwang, and Y. S. Yang, Thin Solid Films **398**, 356 (2001).
[9] K. Wakasugi, M. Tokunaga, T. Sumita, H. Kubota, M. Nagata, and Y. Honda, Physica B **239**, 29 (1997).
[10] C. Stampfl and A. J. Freeman, Phys. Rev. B **67**, 064108 (2003).
[11] *Structure reports*, edited by W. B. Pearson (Oosthoek, Scheltema, and Holkema, Utrecht, 1969), Vol. 35A, p. 121.
[12] N. E. Brese, M. O'Keeffe, P. Rauch, and F. J. DiSalvo, Acta Crystallogr., Sect. C: Cryst. Struct. Commun. **47**, 2291 (1991).
[13] E. Wimmer, H. Krakauer, M. Weinert, and A. J. Freeman, Phys. Rev. B **24**, 864 (1981).
[14] A. Canning, W. Mannstadt, and A. J. Freeman, Comput. Phys. Commun. **130**, 233 (2000).
[15] L. Hedin and B. I. Lundqvist, J. Phys. C **4**, 2064 (1971).
[16] K. Reuter and M. Scheffler, Phys. Rev. B **65**, 035406 (2002).
[17] D. R. Stull and H. Prophet, *JANAF Thermochemical Tables*, 2nd ed., U.S. National Bureau of Standards (U.S. GPO, Washington, D.C., 1971).
[18] L. Hedin, Phys. Rev. **139**, A796 (1965).
[19] D. M. Bylander and L. Kleinman, Phys. Rev. B **41**, 7868 (1990); R. Asahi, W. Mannstadt, and A. J. Freeman, *ibid.* **59**, 7486 (1999).
[20] D. Vogel, P. Krüger, and J. Pollmann, Phys. Rev. B **54**, 5495 (1996); C. Stampfl, C. G. Van de Walle, D. Vogel, P. Kruger, and J. Pollmann, *ibid.* **61**, R7846 (2000).
[21] M. Staedele, M. Moukara, J. A. Majewski, P. Vogl, and A. Görling, Phys. Rev. B **59**, 10 031 (1999).